A new method to compute quasi-local spin and other invariants on marginally trapped surfaces

Michael Jasiulek[*]

Max-Planck-Institut für Gravitationsphysik,
Albert-Einstein-Institut, Golm, Germany

(Dated: June 8, 2009)

Abstract

We accurately compute the scalar 2-curvature, the Weyl scalars, associated quasi-local spin, mass and higher multipole moments on marginally trapped surfaces in numerical 3+1 simulations. To determine the quasi-local quantities we introduce a new method which requires a set of invariant surface integrals, allowing for surface grids of a few hundred points only. The new technique circumvents solving the Killing equation and is also an alternative to approximate Killing vector fields. We apply the method to a perturbed black hole ringing down to Kerr and compare the quasi-local spin with other methods that use Killing vector fields, coordinate vector fields, quasinormal ringing and properties of the Kerr metric on the surface. It even agrees with the spin of approximate Killing vector fields during the phase of perturbed axisymmetry. Additionally, we introduce a new coordinate transformation, adapting spherical coordinates to any two points on the sphere like the two minima of the scalar 2-curvature on axisymmetric trapped surfaces.

PACS numbers: 04.25.Dm, 04.30.Db, 04.70.Bw, 95.30.Sf, 97.60.Lf

---

[*]Electronic address: michael.jasiulek@aei.mpg.de

I. INTRODUCTION

Numerical relativity has undergone a rapid development in the past few years. After the break-through of [1, 2, 3], stable longterm simulations of binary black hole (BBH) systems are common practice, besides waveform modelling, to study the close-to-merger spin precession [4, 5] or to model the final spin [6, 7, 8, 9, 10] of BBH inspirals [11, 12, 13, 14, 15, 16]. Recently extensive investigations have been done concerning the formation process and spin evolution of black holes with accretion disks [17, 18] appearing in fully relativistic simulations of binary neutron stars [19, 20, 21], mixed binaries [22, 23, 24] and rotating neutron star collapse [25, 26, 27, 28].

In these cases accurate numerical techniques to extract the spin of a BH in a gauge invariant manner are required. It is common to obtain a rough approximation of the spin via the quasinormal oscillation extracted from the gravitational waveform after merger, where a perturbed Kerr space-time is assumed. Another approximation scheme is to integrate the radiated angular momentum during the simulation at 'large' coordinate spheres to draw conclusions about the remaining spin of the system given the initial data.

Other methods, as discussed in this paper, use the gauge invariant notation of an apparent horizon (AH) or in more general terms a marginally outer trapped surface (MOTS) which can be located on the spatial slices of the simulation. There gauge invariant spin and mass can be defined, if an axial Killing vector field (KVF) Φ^a is present, as in the case of Kerr. But opposed to the stationary case, the spacetime outside the horizon can be dynamical without spoiling the gauge invariance of these quantities [29, 30, 31, 32]. The invariant quasi-local spin $J[\Phi^j]$ is given by the surface integral (Brown-York form)

$$J[\Phi^j] := -\frac{1}{8\pi} \oint_S \Phi^j K_{ij} s^i dA \,, \tag{1.1}$$

where dA is the 2D area element, K_{ij} the extrinsic curvature of the Cauchy slice and s^i is the outward-pointing surface normal on the MOTS denoted by S. In order to obtain Φ^j the 2D Killing equation has to be solved; if the axisymmetry is perturbed approximate KVFs (aKVFs) have to be calculated [33, 34, 35], for applications in BBH simulations see [11, 16]. Sometimes, due to computational reasons, the effort of finding a KVF or aKVF is not done and coordinate vector fields are instead used to estimate $J[\Phi^j] \approx J[\Phi^j_{\mathrm{cv}}]$, see e.g. [4]. Another common set of methods to determine the spin uses properties of the Kerr solution at the horizon, such as the proper length of the 'equatorial' circumference [36] or the extrema of the scalar 2-curvature [16].

In this paper we present a new, comparatively easy to implement algorithm, which is based on a multipole decomposition of the *rotational* Weyl scalar $\mathrm{Im}\Psi_2$ [37] in the framework of the isolated and dynamical horizon formalism [30, 31, 32]; for reviews see e.g. [31, 38, 39]. The dipole term reads

$$J_1 = -\sqrt{\frac{1}{12\pi}} \frac{A}{4\pi} \oint_S \mathrm{Im}\Psi_2 \, Y^{10}(\chi) \, dA \,, \tag{1.2}$$

where (χ, ϕ) is an invariant coordinate system [37] 'tied' to the axisymmetry, such that J_1 and $J[\Phi^j]$ are identical, and $Y^{10}(\chi)$ is the spherical harmonic $l = 1$, $m = 0$. We circumvent the use of invariant coordinates/KVFs and instead use the averages μ_n [1]of the scalar 2-curvature $^2\mathcal{R}$ and $\mathrm{Im}\Psi_2$ to obtain J_1 and higher multipole moments

$$\mu_n(\bullet) := \langle ((\langle\bullet\rangle - \bullet)^n \rangle \,, \quad \langle\bullet\rangle := \frac{1}{A} \oint_S \bullet \, dA \,, \tag{1.3}$$

---

[1] In statistics μ_n is called the nth *central moment* of the probability distribution of a random variable.

which are well defined, even if the axisymmetry is perturbed and that allow us to benefit from exact numerical integration in order to reduce grid size and numerical error significantly. The invariant surface integrals $\mu_n(^2\mathcal{R})$, $\mu_n(\text{Im}\Psi_2)$ are related to the horizon spin, mass and higher multipole moments by algebraic systems of equations. Where the latter are defined in the presence of an axisymmetry only [37], the μ_n allow to extend them to the perturbed case as a solution of these systems.

In order to minimize numerical errors of $\mu_n(^2\mathcal{R})$, $\mu_n(\text{Im}\Psi_2)$ accurate numerical computations of the curvature components $^2\mathcal{R}$, $\text{Im}\Psi_2$ and the surface triad ^{2}on the horizon are required which is usually given by the Cartesian coordinate *shape function* $h(\theta,\phi) = \sqrt{\delta_{ij}X^iX^j}$ in the simulation, where X^j are the Cartesian coordinates at the 2-surface centered at a point inside the surface. Instead of finite differencing we expand the shape function in terms of a tensor basis to determine Cartesian derivatives off the surface, as commonly used in horizon finding algorithms [40]. But opposed to [40], we use another basis, which is easier to implement, and exact numerical integration to determine the multipole coefficients of $h(\theta,\phi)$, where [40] use minimization to determine the coefficients.

As a further technical novelty we introduce a coordinate remapping which adapts spherical coordinates to the minima of the scalar 2-curvature on the horizon. This coordinate transformation 'roughly' approximates the invariant spherical coordinates, if an axisymmetry is present. In that case the azimuthal coordinate lines yield an axial coordinate vector field to estimate the spin with (1.1), similar to the Cartesian coordinate vector field of [4]. Moreover, a re-interpolation on this new coordinate system can be useful before applying methods aiming to solve the Killing equation, in which finite differencing is involved, like the Killing transport method [33]. Additionally, the axis given by the two minima can be used to define a spin direction, in order to study the close to merger spin precession, as an alternative to the Euclidean spin vector of [4].

We apply the new methods to the AH of a perturbed, ringing BH ^{3}in a 3+1 simulation, where we follow the evolution of spin and mass multipoles until their final Kerr values are reached. It is interesting to compare the angular momentum dipole (1.2) with other spin measures and spin approximants during the evolution.

This paper is organized in the following way. In section II we briefly review numerical methods to find Killing vector fields and approximate Killing vector fields on AHs. In section III we deduce the analytic expressions to determine spin and mass given the geometric properties of an AH in Kerr, such as area, 'equatorial' circumference, extrema of the scalar 2-curvature or the numerically more convenient surface integral we use. Section IV is dedicated to the angular momentum and mass multipole moments on axisymmetric AHs. In particular, we show how these multipole moments are related to the invariant integrals $\mu_n(^2\mathcal{R})$, $\mu_n(\text{Im}\Psi_2)$. In section V we show how to compute the curvature components $^2\mathcal{R}$, Ψ_n and the surface triad accurately. In section VI we explain the setup and initial data of your 3+1 simulation. During the evolution we follow spin, mass and higher multipole moments, compare different methods to measure the spin and test their convergence.

Notation: Indices i,j,k indicate 3D Cartesian components, indices a,b,c label 2D components on the local horizon grid, letters l,m label spherical harmonics. We indicate dimensionless quantities (mass dimension) with a hat, e.g. $\hat{a} = J/m$, $^2\hat{\mathcal{R}} = {}^2\mathcal{R} \cdot A/(8\pi)$, $\text{Im}\hat{\Psi}_2 = \text{Im}\Psi_2 \cdot A/(4\pi)$.

---

^{2} Note that a 'coordinate-induced' surface triad on 'large' coordinate spheres (as for wave extraction via Ψ_4) is given analytically, where the horizon shape in Cartesian coordinates is a deformed 2-sphere and the construction of a surface triad (to obtain for example the Weyl scalars at the horizon) non-trivial.

^{3} We evolve *two puncture* ID. The punctures are close enough to form a common horizon initially.

II. SOLVING THE 2D KILLING EQUATION NUMERICALLY

The induced 2-metric q_{ab} of an ellipsoid S embedded the Euclidean space admits one rotational Killing vector field Φ^a which is a solution of the *Killing equation*

$$\mathcal{L}_\Phi q_{ab} = {}^2D_{(a}\Phi_{b)} = 0\,, \tag{2.1}$$

where ${}^2D$ is the induced covariant derivative on S. The vector field Φ^a is unique up to a constant. In the case of Kerr for example, where $\Phi^a = \partial_\phi$ and ϕ is the Boyer-Lindquist coordinate, it is fixed such that integral curves have affine length of 2π, thus $\phi \in [0; 2\pi]$.

A. Killing Transport Method

Dreyer et al. [33] used the Killing transport method, see appendix of [41], to solve the Killing equation (2.1). Since we apply this method in our simulations, see section VI, we briefly explain it in the following.

The method can be roughly divided into three steps: 1. determine a single vector of the KVF at a point on an arbitrary loop on S, 2. spread this vector throughout the whole surface, 3. normalize the whole KVF by normalizing an arbitrary integral curve to have affine length of 2π. The first two steps require the *Killing transport equation*

$$\begin{aligned} c^a\,{}^2D_a\Phi_b &= c^a L\,{}^2\varepsilon_{ab} \\ c^a\,{}^2D_a(L\,{}^2\varepsilon_{bc}) &= c^a {}^2R^d{}_{cba}\Phi_d\,, \end{aligned} \tag{2.2}$$

where ${}^2\varepsilon_{ab}$ denotes the Levi-Cevita tensor and ${}^2R^d{}_{cba}$ the 2D Riemann tensor. This equation holds for any function L and vector field c^a on S as long as Φ^a is the KVF. On the other hand, assume that Φ_b and L were unknown, pick a loop, e.g. the equator c_e, $(\theta = \pi/2, \phi)$ of a spherical coordinate system, pick a point, e.g. P, $(\theta = \pi/2, \phi = 0)$ and identify $c^a := \partial_\phi$ [4], then (2.2) becomes an ODE for the unknown $(\Phi_1(\phi), \Phi_2(\phi), L(\phi))$ along c_e. This defines a linear operator for 3-vectors at P. If we pick three arbitrary, linear independent initial vectors at P, transport (2.2) them along the loop to P, we obtain a 3×3 matrix presentation of this operator. Two components of its eigenvector are the KVF at P (1. step), the third is the auxiliary function L at P. At next this 3-vector is transported (2.2) along coordinate lines all over S, setting $c^a = \partial_\phi$ or $c^a = \partial_\theta$ respectively (2. step). Where the transportation equation (2.2) by construction 'conserves' the Killing property. The last step is to normalize the KVF (3. step), where we have to solve the ODE $\partial_t\theta = \Phi^1(\theta, \phi)$, $\partial_t\phi = \Phi^2(\theta, \phi)$, Φ_0^a, where the initial vector Φ_0^a is arbitrary, to obtain an integral curve and normalize such that the curve parameter $t \in [0; 2\pi]$.

B. Approximate Killing Vector Fields

If the ellipsoid S is slightly deformed, no exact solution of (2.1) exists. But one could try to find a 'best match' which minimizes a certain norm of the l.h.s. of (2.1) on S. Such vector fields are often denoted as *approximate Killing vector fields* (aKVF). Opposed to KVFs there is no unique definition of aKVFs. Dreyer et al. [33] could show that the Killing transport method is still

---

[4] The resulting KVF is independent of the initial loop, initial point and curve parameter.

applicable to yield a 'well matching' aKVF. But one has to be aware that the final vector field will not be anymore independent of the particular loops of transportation. Although this effect may be negligible for practical applications, e.g. [4, 7] , if the departure from axisymmetry is 'small'.

We found it useful to adapt the coordinate system on the horizon before applying the Killing transport method such that the azimuthal transport revolves the minima of the scalar 2-curvature [5], see appendix B. Another approach to find an approximate Killing vector field has been given by [34]. They use a variational principle to minimize the 'non-symmetric' features of the vector field. A similar method can be found in the appendix of [42], for an application to a BBH simulation see [16]. Caudill et al. [43] consider the conformal Killing equation in order to define an aKVF. Recently Beetle [44] pointed out that Cook's [34] approach is closely related to an older proposal by Matzner [35], where the aKVF is the solution of an eigenvalue problem. An outstanding question is still the normalization of these aKVFs. An interesting new idea has been given in the appendix of [42], where the aKVF is normalized to a particular surface integral instead of a single integral curve.

C. Coordinate Vector Fields

If the coordinates are conveniently adapted to the metric manifold, the coordinate vectors automatically generate symmetries, such as the Boyer-Lindquist coordinate vectors ∂_t and ∂_ϕ in a Kerr spacetime. If a coordinate vector field is known to be 'close' to a KVF like in the *adapted spherical coordinates* $(\theta_{\mathrm{asc}}, \phi_{\mathrm{asc}})$, see appendix B,

$$\Phi^a_{\mathrm{asc}} = \partial_{\phi_{\mathrm{asc}}} \, , \tag{2.3}$$

one can use it to estimate the spin $J[\Phi^j] \approx J[\Phi^j_{\mathrm{asc}}]$ with (1.1), see the application in section VI.

Similarly Campanelli et al. [4] use the three rotational Killing vectors of Euclidean space in Cartesian coordinates

$$\Phi^{i[j]}_{\mathrm{cc}} = (x^k - C^k)\epsilon^{ij}{}_k \, , \, j = 1, 2, 3 \, , \tag{2.4}$$

where $\epsilon^{ij}{}_p \delta^{pk} = \epsilon^{ijk}$ is the flat space Levi-Cevita tensor and C^j a point inside S, to define a Euclidean spin vector $(J[\Phi^{i[1]}_{\mathrm{cc}}], J[\Phi^{i[2]}_{\mathrm{cc}}], J[\Phi^{i[3]}_{\mathrm{cc}}])$ and together with (1.1) to estimate $J[\Phi^i] \approx J[\Phi^i_{\mathrm{cc}}]$, where $J[\Phi^i_{\mathrm{cc}}]$ denotes the Euclidean norm of this vector which allows them to study the spin precession in a BBH inspiral and to estimate the final spin after merger. Referring to [4] this Euclidean spin vector reproduces the Bowen-York spin parameters of the conformally flat initial data and for the final black hole $|J[\Phi^j] - J[\Phi^j_{\mathrm{cc}}]| \ll 1$.

III. INVARIANTS OF THE HORIZON IN KERR

If an AH, say, detected in a 3+1 simulation, is approximated to be in a slice of Kerr, the numerical extraction of the black hole spin given the ADM or BSSN evolution variables at the AH is relieved and it can be avoided to solve the Killing equation (2.1). The Kerr spacetime is uniquely defined by two invariant numbers, like spin and mass (J, m), like 'equatorial' circumference [6] and area $(L(c_e), A)$ of the BH surface, see [36], or an extremum of the scalar 2-curvature

---

[5] An ellipsoid has two minima of the scalar 2-curvature which coincide with the minima of the KVF, given by the symmetry axis of the body.

and area $(^2\mathcal{R}_{\text{ext}}, A)$, see [42]. Each pair is related to the other by the Kerr metric and we can choose the numerically most convenient one. In order to benefit from exact numerical integration we select the invariants $(\mu_2(^2\hat{\mathcal{R}}), A)$, see (1.3). The explicit algebraic expressions relating $J \leftrightarrow L(c_e) \leftrightarrow {}^2\mathcal{R}_{\text{ext}} \leftrightarrow \mu_2(^2\hat{\mathcal{R}})$ $(\leftrightarrow \mu_2(\text{Im}\hat{\Psi}_2))$ are derived in the following.

Any axisymmetric 2-metric q_{ab} can be put in the compact form

$$dq^2 = \frac{A}{4\pi}\left(\frac{1}{f(\chi)}d\chi^2 + f(\chi)d\phi^2\right). \tag{3.1}$$

For the 2-surface of a Kerr black hole $f(\chi)$, see [45], is given by

$$f(\chi) = \frac{1-\chi^2}{1-\hat{\beta}^2(1-\chi^2)}, \quad \chi := \cos\theta, \tag{3.2}$$

where $\hat{\beta} \in [0; 1/\sqrt{2}]$ is called the *Kerr distortion parameter* and (θ, ϕ) are the Boyer-Lindquist spherical coordinates. The distortion parameter $\hat{\beta}$ is related to the more familiar dimensionless spin parameter $\hat{a} = a/m = J/m^2$ by

$$\hat{\beta}^2 = \frac{1}{2}\left(1 - \sqrt{1-\hat{a}^2}\right), \tag{3.3}$$

to Kerr spin J and mass m [7] by

$$J = \frac{A}{8\pi}\sqrt{\frac{1-\sqrt{1-\hat{a}^2}}{1+\sqrt{1-\hat{a}^2}}} = \frac{A}{8\pi}\frac{\hat{\beta}}{\sqrt{1-\hat{\beta}^2}} = \frac{A}{8\pi}\hat{c}, \quad m = \frac{1}{2}\sqrt{\frac{A}{4\pi(1-\hat{\beta}^2)}}. \tag{3.4}$$

Smarr [45] pointed out the analog of the surface of rotating material bodies to the black hole horizon, where the equatorial circumference increases as the body spins up. The equatorial circumference for the Kerr horizon is given by integrating (3.1) along the maximum of $^2\mathcal{R}$ which is the curve $(\chi = 0, \phi)$,

$$L(c_e) = \oint_0^{2\pi}\sqrt{\frac{A}{4\pi}f(\chi = 0)}\,d\phi = \sqrt{\frac{A\pi}{1-\hat{\beta}^2}} = 4\pi m. \tag{3.5}$$

For the numerical application in arbitrary coordinates this is only useful, if the curve c_e is known to overlap with a coordinate line. If this is not the case the extrema of $^2\mathcal{R}$ are a practical alternative, see [16, 42]. The scalar 2-curvature of q_{ab} (3.1) is

$$^2\mathcal{R} = -\frac{8\pi}{A}\frac{1}{2}f''(\chi) \quad \rightarrow \quad {}^2\hat{\mathcal{R}} = -\frac{1}{2}f''(\chi), \tag{3.6}$$

with extrema at $\chi_{\text{min}} = 1; -1$, $\chi_{\text{max}} = 0$. We obtain

$$^2\hat{\mathcal{R}}_{\text{max}} = \frac{1}{(1-\hat{\beta}^2)^2}, \quad {}^2\hat{\mathcal{R}}_{\text{min}} = 1 - 4\hat{\beta}^2. \tag{3.7}$$

---

[6] This is the curve c_e along the maximum of $^2\mathcal{R}$ in Kerr.

[7] For completeness note that $m_{\text{irr}} = R_{\text{areal}}/2$ is the *irreducible mass* and $R_{\text{areal}} = \sqrt{A/(4\pi)}$ the *areal radius*.

A. An invariant surface integral in Kerr

If the scalar 2-curvature has been computed on a finite grid, interpolation is required to obtain the extrema. This is not necessary if the following surface integrals are employed

$$\mu_2\left(^2\hat{\mathcal{R}}\right) := \left\langle \left(\left\langle ^2\hat{\mathcal{R}}\right\rangle - ^2\hat{\mathcal{R}}\right)^2 \right\rangle, \quad \left\langle ^2\hat{\mathcal{R}}\right\rangle := \frac{1}{A}\oint_S {}^2\hat{\mathcal{R}}\, dA. \tag{3.8}$$

Moreover, the numerical error of $\mu_2(^2\hat{\mathcal{R}})$ benefits from averaging over all points on the grid and exact numerical integration can be used. With the normalization of (3.6) the average $<^2\hat{\mathcal{R}}>_{\text{grid}}= 1 + \epsilon_{\text{numerical}}$ for any 2-metric computed on a finite grid on S according to the Gauss-Bonnet theorem. For Kerr the integral appearing in (3.8) is taken over a rational function in χ. We obtain

$$\mu_2(^2\hat{\mathcal{R}}) = \frac{-15 - 70\hat{c}^2 + 128\hat{c}^4 + 70\hat{c}^6 + 15\hat{c}^8}{80(1+\hat{c}^2)} + \frac{3(1+\hat{c}^2)^4}{16}\frac{\arctan(\hat{c})}{\hat{c}}, \tag{3.9}$$

where $\hat{c}$ is given by (3.4). In the numerical simulations of section VI we compute $(\mu_2(^2\hat{\mathcal{R}}), A)$ on the AH and calculate the corresponding (J, m) with (3.9) and (3.4). Where we assume that the AH is in a slice of Kerr, which is a rough approximation for the common horizon directly after the merger of two black holes, but as soon as the 'non-Kerr' features have vanished below the numerical error this method yields an accurate measure of the final black hole spin and mass.

Note that for Kerr $\text{Im}\hat{\Psi}_2 = -\frac{1}{4}g''(\chi)$, $g(\chi) := \frac{(1+\hat{c}^2)^2}{\hat{c}(1+\hat{c}^2\chi^2)}$, see [46] and some algebra, which means $\mu_1(\chi\cdot\text{Im}\hat{\Psi}_2) = \hat{c}$. That is inconvenient in application, since the Boyer-Lindquist coordinate $(\chi = \cos\theta)$ explicitly appears. For $\mu_2(\text{Im}\hat{\Psi}_2)$ we obtain a similar expression to (3.9) which is $\mu_2(\text{Im}\hat{\Psi}_2) = \frac{-15+170\hat{c}^2+112\hat{c}^4+70\hat{c}^6+15\hat{c}^8}{320(1+\hat{c}^2)} + \frac{3(1+\hat{c}^2)^4}{64}\frac{\arctan(\hat{c})}{\hat{c}}$. Therefore, we do not expect to get more information by extracting $\hat{c}$ from $\mu_2(\text{Im}\hat{\Psi}_2)$ or $\mu_2(^2\hat{\mathcal{R}})$ or higher μ_n but rather from the whole sets $\mu_n(\text{Im}\hat{\Psi}_2)$, $\mu_n(^2\hat{\mathcal{R}})$ and the procedure explained in the next section (when applied to a perturbed axisymmetric horizon).

IV. INVARIANTS OF AXISYMMETRIC ISOLATED HORIZONS

For the calculations in the last section to be reasonable when applied to an AH found in a numerical simulation, we had to assume that the detected 2-surface was in a slice of Kerr. We relax this condition and allow the spacetime to be dynamical in the vicinity of the horizon which we assume to be an axisymmetric *isolated horizon* (IH) [29, 30]. On the horizon in Kerr all multipole moments are necessarily given by spin and mass, therefore higher moments contain no extra information. This is in general not the case on an axisymmetric IH, where an infinite set of independent multipole moments permits more complexity, see [37].

At first the axisymmetry has to be exploited to define an invariant coordinate system (χ, ϕ) for which the 2-metric has the form (3.1), ∂_ϕ is the KVF and the zonal harmonics $\{Y^{l0}(\chi)\}$ represent an orthonormal basis $\oint_S Y^{l0}(\chi)Y^{l'0}(\chi)dA = \frac{A}{4\pi}\delta^{ll'}$. At next note that, as valid for Kerr, the Weyl scalar Ψ_2 is gauge invariant on IHs without matter fields, in both cases $\text{Re}\Psi_2 = -1/4\,^2\mathcal{R}$ holds

and the dimensionless IH multipole moments $\hat{I}_l$, $\hat{L}_l$ are defined by

$$\hat{I}_l := \oint_S 1/4\,^2\mathcal{R}(\chi)Y^{l0}(\chi)\,dA\,, \qquad\qquad \hat{L}_l := -\oint_S \text{Im}\Psi_2(\chi)Y^{l0}(\chi)\,dA\,. \qquad (4.1)$$

$$^2\mathcal{R}(\chi) = 4\cdot\frac{4\pi}{A}\sum_{l=0}^{\infty}\hat{I}_l\,Y^{l0}(\chi)\,, \qquad\qquad \text{Im}\Psi_2(\chi) = -\frac{4\pi}{A}\sum_{l=0}^{\infty}\hat{L}_l\,Y^{l0}(\chi)\,. \qquad (4.2)$$

Note that for Kerr $J\cdot 8\pi/A = \hat{c} = \sqrt{1/(3\pi)}\,\hat{L}_1$ and for an IH $J[\Phi^j]\cdot 8\pi/A = \sqrt{1/(3\pi)}\,\hat{L}_1$, where Φ^j is the KVF corresponding to (χ,ϕ) and $J[\Phi^j]$ given by (1.1). Therefore, the curvature component $\text{Im}\Psi_2$ is sometimes called *rotational* Weyl scalar and the $\hat{L}_l$ *angular momentum* multipole moments, all vanish in the absence of spin. The invariants $\hat{I}_l$, $\hat{L}_l$ are subject to certain algebraic constraints such that $\hat{I}_0 = \sqrt{\pi}$ (Gauss-Bonnet), that the mass dipole $\hat{I}_1$ and the angular momentum monopole $\hat{L}_0$ vanish [8]. If the 2-metric (3.1) admits a reflection symmetry as for Kerr $f(\chi) = f(-\chi)$, see (3.2), all odd $\hat{I}_l$ and even $\hat{L}_l$ vanish, too.

A. The invariants μ_n on axisymmetric isolated horizons

In analogy to subsection III A we want to use the invariants $\mu_n(^2\hat{\mathcal{R}})$, $\mu_n(\text{Im}\hat{\Psi}_2)$, see (1.3), to determine the IH multipole momenta because a direct computation of the integrals $\hat{I}_n$, $\hat{L}_n$ (4.1) would require the knowledge of the invariant coordinates and thus the KVF Φ^j (then the spin $J[\Phi^j]$ could be directly computed (1.1)). Therefore we calculate the algebraic relations between the $\mu_n(^2\hat{\mathcal{R}})$, $\mu_n(\text{Im}\hat{\Psi}_2)$ and the $\hat{I}_n$, $\hat{L}_n$ by inserting (4.2) into (1.3)

$$\mu_n\!\left(^2\hat{\mathcal{R}}\right) = \left\langle\left(1-2\sum_{l=0}^{l_{\max}^I}\hat{I}_l\,Y^{l0}(\chi)\right)^n\right\rangle\,, \qquad n = 2,3,...,n_{\max}^I\,, \qquad (4.3)$$

$$\mu_n\!\left(\text{Im}\hat{\Psi}_2\right) = \left\langle\left(0+\sum_{l=0}^{l_{\max}^L}\hat{L}_l\,Y^{l0}(\chi)\right)^n\right\rangle\,, \qquad n = 2,3,...,n_{\max}^L\,, \qquad (4.4)$$

where we assume that $^2\hat{\mathcal{R}}$, $\text{Im}\hat{\Psi}_2$ are given by finite sets of multipole moments up to $l_{\max}^I$, $l_{\max}^L$. We obtain [9]

$$\mu_n\!\left(^2\hat{\mathcal{R}}\right) = \sum_{m=0}^{n}\binom{n}{m}(-2)^m\sum_{|K_{l_{\max}}|=m}\binom{m}{K_{l_{\max}}}(\hat{I}_-)^{K_{l_{\max}}}\left\langle(Y^{-0})^{K_{l_{\max}}}\right\rangle\,, \qquad (4.5)$$

$$\mu_n\!\left(\text{Im}\hat{\Psi}_2\right) = \sum_{|K_{l_{\max}}|=n}\binom{n}{K_{l_{\max}}}(\hat{L}_-)^{K_{l_{\max}}}\left\langle(Y^{-0})^{K_{l_{\max}}}\right\rangle\,, \qquad n = 2,3,...,n_{\max}\,, \qquad (4.6)$$

where $K_{l_{\max}} = (k_1,k_2,...,k_{l_{\max}})$ is a multi-index of length $l_{\max}$, $\binom{k}{k_1,k_2,...}$ is the multinomial coefficient and $(\hat{I}_-)^{K_{l_{\max}}}\left\langle(Y^{-0})^{K_{l_{\max}}}\right\rangle = (\hat{I}_1)^{k_1}(\hat{I}_2)^{k_2}...\left\langle(Y^{10})^{k_1}(Y^{20})^{k_2}...\right\rangle$. The integers $n_{\max}^I$, $n_{\max}^L$ match the numbers of non-trivial $\hat{I}_n$, $\hat{L}_n$ given by the algebraic constraints mentioned earlier and

---

[8] Therefore, the invariant coordinates are sometimes called 'center of mass frame' of the IH.
[9] Here the indices I, L in $l_{\max}^I$, $l_{\max}^L$, $n_{\max}^I$, $n_{\max}^L$ are omitted.

$l_{\max}^I, l_{\max}^L$. The coefficients $\langle (Y^{\cdot 0})^{K_{l_{\max}}} \rangle$ are integrals over products of (zonal) spherical harmonics. They are given by the associated Clebsch-Gordan coefficients and higher order generalizations.

Consider the following example. In a simulation of a perturbed Kerr spacetime we locate the AH and compute the surface integrals $\mu_n(^2\hat{\mathcal{R}})$, $\mu_n(\text{Im}\hat{\Psi}_2)$ to $n_{\max} = 6$. Where we assume that the 2-surface is a cross-section of an IH with reflection- and axisymmetric 2-metric. Then the algebraic systems (4.3), (4.4) become

$$\mu_n\left(^2\hat{\mathcal{R}}\right) = \left\langle \left(1 - 2(\sqrt{\pi}Y^{00} + \sum_{l=2,4,6,8}\hat{I}_l Y^{l0}) + \mathcal{O}_I\right)^n \right\rangle, \, n = 2,3,4,5,6 \qquad (4.7)$$

$$\mu_n\left(\text{Im}\hat{\Psi}_2\right) = \left\langle \left(\sum_{l=1,3}L_l Y^{l0} + \mathcal{O}_L\right)^n \right\rangle, \, n = 2,4,6 \,, \qquad (4.8)$$

which we solve for $\hat{I}_2$, $\hat{I}_4$, $\hat{I}_6$, $\hat{I}_8$, $\mathcal{O}_I$ and $\hat{L}_1$, $\hat{L}_3$, $\mathcal{O}_L$, where $\mathcal{O}_I$, $\mathcal{O}_L$ are constants accounting for the truncation of the expansions. Among the solutions we pick the one that is real and closest to the corresponding Kerr value or, if no guess for that value is available, we pick the real solution with $-\hat{I}_2 > \hat{I}_4 > -\hat{I}_6 > \mathcal{O}_I$ and $\hat{L}_1 > -\hat{L}_3 > \mathcal{O}_L$. If we were only interested in $\hat{L}_1$ and $\mathcal{O}_L$, two surface integrals $\mu_2(\text{Im}\hat{\Psi}_2)$, $\mu_4(\text{Im}\hat{\Psi}_2)$ would be enough.

In order to attribute a physical interpretation to the $\hat{I}_l$, $\hat{L}_l$, in analogy to electro dynamics, dimensionfull factors can be added, see [37]. Here we require

$$J_1 = \sqrt{\frac{1}{12\pi}} \frac{A}{4\pi} \hat{L}_1 \,. \qquad (4.9)$$

Then $J[\Phi^j] = J_1$ holds for the KVF Φ^j corresponding to (χ, ϕ).

The surface integrals $\mu_n(\text{Im}\hat{\Psi}_2)$ are well defined even in the perturbed axisymmetric case and allow us to extend the concept of IH multipole moments, in analogy to aKVFs which are generalizations of KVFs, where no exact solution of the Killing equation exists. Opposed to the conciderations of the last subsection, we take more information about the horizon geometry into account, than extracting the spin from a single μ_n only and modelling the horizon with Kerr.

V. ACCURATE COMPUTATION OF $^2\mathcal{R}$, Ψ_2 ON THE AH

In this section we will show how to compute the curvature components $^2\mathcal{R}$ and Ψ_2 accurately, where we assume that the 3+1 evolution variables [10]extrinsic 3-curvature K_{ij}, 3-metric γ_{ij} (together with $\partial_i K_{jk}$, $\partial_i \gamma_{jk}$, $\partial_i \partial_j \gamma_{kk'}$) and the horizon coordinate shape X^j are given on a Cartesian grid. The accurate calculation of curvature components on a deformed 2-sphere in a Cauchy slice is a common problem in numerical relativity which appears in horizon finding algorithms. Therefore, the new methods introduced in this paper could be easily implemented as an extension of existing horizon finding routines. Various methods have been tried to discretize the necessary spatial derivatives $\partial_j h$, $\partial_i \partial_j h$ by finite differencing, finite element, pseudo-spectral and spectral methods, using squared (θ, ϕ) grids or multipatch grids, for a review see [47]. Our approach is motivated by the work of [40]. There a spectral decomposition of the coordinate shape function

---

[10] They can be easily assembled from the BSSN evolution variables.

9

$h(\theta, \phi)$ is being used to compute Cartesian derivatives. The 1st derivatives $\partial_j h$ are necessary to obtain a surface triad $\{s^i, u^j, v^k\}$ (required to compute the Weyl scalars) and the 2nd derivatives $\partial_i \partial_j h$ to obtain the extrinsic 2-curvature ${}^2 K_{ij}$ of S embedded into the Cauchy slice (additionally required to compute the scalar 2-curvature).

If we parametrize the AH with spherical coordinates, the embedding $X^j(\theta, \phi)$ into the Cartesian grid is

$$X^j(\theta, \phi) = h(\theta, \phi)\, n^j + C^j, \tag{5.1}$$

where C^j is a coordinate location inside the horizon (for example the coordinate centroid), n^j the Cartesian radial unit vector $n^j = \frac{1}{r} x^j$, $r = \sqrt{\delta_{ij} x^i x^j}$ and x^j are Cartesian coordinates.

A. Spectral decomposition

To compute spatial derivatives one could decompose $h(\theta, \phi)$ into

$$h(\theta, \phi) = \sum_{l=0}^{l_{\max}} \sum_{m=l}^{-l} [h]^{lm} Y^{lm}(\theta, \phi), \tag{5.2}$$

where $[h]^{lm}$ are the expansion coefficients and Y^{lm} the spherical harmonics. The evaluation of $\partial_j Y^{lm}(\theta, \phi)$ would require the Jacobian to transform between spherical and Cartesian coordinates. This is inconvenient for the numerical application, since the Jacobian is singular at the spherical coordinate poles.

Therefore, [40] take a tensor basis which is build of the radial unit vector $n^i(x^j) = x^j/r$ and thus defined in Cartesian coordinates (and easily parametrized with any other local coordinate system on the 2-surface, e.g. spherical $n^i(\theta, \phi) = (\sin\theta\cos\phi, \sin\theta\sin\phi, \cos\theta)$ or stereographic coordinates $n^j(u, v) = (2u, 2v, u^2 + v^2 - 1)/(1 + u^2 + v^2))$,

$$h = \sum_{l=0}^{l_{max}} [h]^{K_l} N_{K_l}, \tag{5.3}$$

where K_l is again a multi-index of length l and the tensor products $N_{K_l} = n_{k_1} n_{k_2} \ldots n_{k_l}$ are symmetric tracefree tensors (STF) of Euclidean space, the notation is adapted from [48]. If the coefficients of the expansion (5.2) are known, they can be translated to obtain the expansion (5.3), for how to $[h]^{lm} \leftrightarrow [h]^{K_l}$ see [40]. The partial derivative of the tensor product $\partial_j N_{K_l}$ consists of the derivatives $\partial_i n_j = (\delta_{ij} - n_i n_j)/r$. In detail the implementation of the STF tensors and its derivatives is a bit cumbersomely but straight forward.

We use another basis of the harmonics instead $(\delta_{ij} n^i \mathcal{N}^j)^l$, where $\mathcal{N}^j$ is a constant complex Euclidean null vector $(\mathcal{N}_j \mathcal{N}^j) = 0$, $\mathcal{N}^j \neq 0$, see Sec.11.5.1., Vol.II [49] or [50]. The expression $(n_j \mathcal{N}^j)^l$ is a homogeneous harmonic polynomial of Euclidean space of order l, therefore $\Delta_{\text{flat}}(n_j \mathcal{N}^j)^l = 0$. The radial vector n^j defines a restriction of the polynomial to the unit sphere $x^i x^j \delta_{ij} = 1$. It is known that such restrictions are eigenfunctions of the Laplacian of the induced metric (this applies to any embedding of S^2 into Euclidean space, e.g. an ellipsoid). On the unit sphere this implies $\Delta_\circ (n_j \mathcal{N}^j)^l = l(l + 1)(n_j \mathcal{N}^j)^l$, where $\Delta_\circ$ is the Laplacian of the standard spherical 2-metric. This holds for any null vector $\mathcal{N}^j$. In order to span each l-eigenspace of $\Delta_\circ$ with $2l + 1$ linear independent eigenfunctions we define a list of null vectors

$$\mathcal{N}^j_{[lm]} = (i\sin(m a_l), i\cos(m a_l), 1), \quad a_l = \frac{2\pi}{2l + 1}, \quad m = -l, \cdots, l, \tag{5.4}$$

10

where the roots of unity have been used such that the $\mathcal{N}^j_{[lm]}$, have the Euclidean norm $\mathcal{N}_j \mathcal{N}^j = -|e^{i\frac{2\pi m}{2l+1}}|^2 + 1$. Now we can define the new basis $\Phi^{lm} := (n_j \mathcal{N}^j_{[lm]})^l$ and decompose h into

$$h = \sum_{l=0}^{l_{\max}} \sum_{m=l}^{-l} [h]^{lm}_{\mathcal{N}} \, (n_j \mathcal{N}^j_{[lm]})^l \,. \tag{5.5}$$

The Φ^{lm}, $m = -l, \cdots, l$ are not orthogonal in each l-eigenspace but across different eigenspaces. They are related to the standard basis by

$$Y^{lm} = B^{lm} \sum_{m'=-l}^{l} \Phi^{lm'} e^{-i\,m'\,m\,a_l}, \tag{5.6}$$

$$\Phi^{lm} = \frac{1}{2l+1} \sum_{m'=-l}^{l} \frac{Y^{lm'}}{B^{lm'}} e^{i\,m'\,m\,a_l}, \tag{5.7}$$

$$B^{lm} = (-1)^m \frac{1}{l!} \sqrt{\frac{(l+m)!(l-m)!}{4\pi(2l+1)}}\,. $$

and we can transform the coefficients $[h]^{lm} \leftrightarrow [h]^{lm}_{\mathcal{N}}$. Derivatives of the new basis are given by

$$\partial_k \Phi^{lm} = (n_j \mathcal{N}^j)^{l-1} l \, (\partial_k n_j \mathcal{N}^j) \tag{5.8}$$

$$\partial_k \Phi^{lm} = (n_j \mathcal{N}^j)^{l-1} l \frac{1}{r} \left(\mathcal{N}_k - n_k n_j \mathcal{N}^j \right) \,, \tag{5.9}$$

and similarly for higher derivatives $\partial_i \partial_j \Phi^{lm}$.

B. Surface triad

Now we have the Cartesian derivatives $\partial_j h$, $\partial_j \partial_i h$ at hand and are able to compute the outward pointing surface normal $s^j = \gamma^{jk} s_k$

$$s_j = \lambda(n_j - \partial_j h), \quad \lambda = 1/\sqrt{\gamma^{ij}(n_i - \partial_i h)(n_j - \partial_j h)}\,. \tag{5.10}$$

In order to complete the surface triad $\{s^i, u^j, v^k\}$ we set $u^j = \frac{1}{\gamma_{ik}\partial_\theta X^i \partial_\theta X^k} \partial_\theta X^j$ and $v^k = \varepsilon^{ijk} s_i u_j$, where $\varepsilon^{ijk} = \|\gamma\|^{-1/2}[123]^{ijk}$ is the spatial Levi-Civita tensor and $[123]^{ijk}$ the pure alternating symbol.

C. Extrinsic and intrinsic 2-Curvature

The extrinsic 2-curvature $^2K_{ij}$ of S embedded into the Cauchy slice is given by

$$^2K_{ij} = D_i s_j - s_i s^k D_k s_j \,, \tag{5.11}$$

where the second derivatives $\partial_j \partial_k h$ are required and the Christoffel symbols associated to the 3-metric. Then the intrinsic 2-curvature $^2\mathcal{R}$ is given by Gauss' *theorema egregium*

$$^2\mathcal{R} = \mathcal{R} - 2R_{ij} s^i s^j + {}^2\mathcal{K}^2 - {}^2K^{ij}\,{}^2K_{ij} \,, \tag{5.12}$$

where $^2\mathcal{K} = {}^2K_{ij} q^{ij}$ and $q^{ij} = \gamma^{ij} - s^i s^j$ is the induced 2-metric in Cartesian components (also required to raise the indexes of $^2K_{ij}$ in the last summand on the r.h.s. of (5.12)).

11

D. Area Element

The computation of surface integrals on the AH requires the area element $dA = \sqrt{\det q_{ab}}\, d\theta d\phi$, where we need the induced 2-metric in local coordinates

$$q_{ab} = \partial_a X^j \partial_b X^k \gamma_{jk}\,, \tag{5.13}$$

here X^j has been defined in (5.1), for an alternative see appendix of [40].

E. Ψ_2 and other Weyl scalars

To obtain mass and angular momentum multipoles (4.1) an accurate computation of Ψ_2, given the 3+1 evolution variables, is requried. Additionally, we want to follow the constraints $\Psi_0 = 0$ and $\Psi_1 = 0$ which hold for Kerr and on IHs [29] in the simulation of section VI. The *electric* E_{ij} and *magnetic* B_{ij} parts of the Weyl tensor C_{ijkl} w.r.t. time-like normal $\tilde{n}^\mu$ of the Cauchy slice are

$$E_{ij} \equiv -C_{ijkl}\tilde{n}^k\tilde{n}^l = -R_{ij} + K_i{}^k K_{kj} - \mathcal{K}\, K_{ij}\,, \tag{5.14}$$
$$B_{ij} \equiv - \star C_{ijkl}\tilde{n}^k\tilde{n}^l = -\varepsilon_i{}^{kl} D_k K_{lj}\,. \tag{5.15}$$

We further project E_{ij}, B_{ij} onto the surface triad $\{s^i, u^j, v^k\}$ and obtain the Weyl scalars, see [51, 52],

$$\Psi_2 = -\frac{1}{2}(E_{jk} - iB_{jk})s^j s^k\,, \tag{5.16}$$

$$\Psi_0 = -(E_{jk} - iB_{jk})m^j m^k\,, \tag{5.17}$$

$$\Psi_1 = -\frac{1}{\sqrt{2}}(E_{jk} - iB_{jk})m^j s^k, \tag{5.18}$$

where $m^j = \frac{1}{\sqrt{2}}(u^j - iv^j)$.

We monitor the dynamics of the AH during the evolution in section VI by computing the dimensionless surface integrals

$$\hat{\psi}_0 = \oint_S |\Psi_0|\, dA, \quad \hat{\psi}_1 = \oint_S |\Psi_1|\, dA, \quad \hat{\psi}_2 = \left| \frac{1}{8\pi} \oint_S 4\mathrm{Re}\,\Psi_2\, dA + 1 \right|\,, \tag{5.19}$$

which vanish for a MOTS in a slice of Kerr or an IH.

VI. NUMERICAL EVOLUTION AND INITIAL DATA

In order to test and compare the new techniques we applied them to an AH of a perturbed ringing BH in a 3+1 simulation which as been carried out using the CCATIE code [11]. This is a 3D finite differencing code based on the Cactus Computational Toolkit [53]. The CCATIE code provides a collection of modules (*thorns*) which allow us to use *puncture initial data* [54] with the TwoPunctures thorn [55], to do the time evolution of this initial Cauchy slice with the BSSN evolution system [56, 57, 58], to set proper gauge conditions (where we used 1+log slicing and the hyperbolic gamma-driver condition as in [59]), to successively refine the Cartesian mesh with several nested static boxes around the AH (where we used the Carpet AMR driver [60]) and to locate

the horizon every few time steps during the evolution [61]. The horizon finding thorn [11] provides the shape function $h(\theta, \phi)$ which is being used by a separate thorn to interpolate (4th-order Lagrange) all necessary 3+1 evolution variables onto the spherical grid, to accurately compute the curvature components $^2\mathcal{R}$, $\mathrm{Im}\Psi_2$ at the horizon (see section V) and, finally, to determine the associated quasi-local IH multipole moments using the surface integrals (1.3).

In addition to the angular momentum dipole $J_1(\mu_{2,4,6}(\mathrm{Im}\hat{\Psi}_2), A)$ [12], we compare the spin with four other methods: 1. $J[\Phi^j_{\mathrm{kt}}]$ using the Killing transport method of subsection II A to obtain the KVF Φ^j_{kt} and equation (1.1) in adapted spherical coordinates (see appendix A), 2. $J[\Phi^j_{\mathrm{cc}}]$ and $J[\Phi^j_{\mathrm{asc}}]$, where we approximate the KVF with the coordinate vector fields of subsection II C, 3. $J(\mu_2(^2\hat{\mathcal{R}}), A)$, where we use a single surface integral and the formula (3.9) (assuming closeness to Kerr) to extract the spin.

A. Initial Data and Grid Parameters

In order to model the common horizon after the coalescence of an arbitrarily aligned BBH system we chose as a non-trivial initial configuration a misaligned spinning puncture with a nearby smaller non-spinning companion puncture, where the common horizon is already present on the initial slice. The Bowen-York parameters of the first puncture are $m_1 = 0.8M$, $|s_1| = 0.3M^2$ with orientation $(\theta_{s_1} = 0.6, \phi_{s_1} = 0.4)$ in the Cartesian grid. And for the second puncture we set $m_2 = 0.2M$, $s_2 = 0$.

We evolve the initial data 4th-order in space and time with the Cartesian grid resolutions $\Delta x = 0.048M, 0.035M, 0.025, 0.02M$ (finest AMR resolutions) and use three different spherical grid resolutions $N_\theta \times N_\phi = N_S = 480, 1104, 4900$, where N_S is the total number of grid points on the surface and $N_\phi = 2N_\theta$ (where the 6-patch grid of the horizon finder and the spherical grid are kept at the same resolution). The spectral resolution for the expansion of the shape function h is fixed to $l_{\max} = 10$.

B. Numerical Evolution

1. Monitoring the Isolation Constraints

To monitor the dynamics on the horizon we computed the surface integrals (5.19) shown in figure 1 (for Kerr $\hat{\psi}_{0,1,2} = 0$). On the left we see the typical exponentially damped oscillation of the *radiative* Weyl scalars Ψ_0, Ψ_1 which are (after an initial burst $\hat{\psi}_{0,1} \ll 1$) given by a superposition of several quasinormal-modes, predominately $l = 2$ modes, that have been excited by the specific initial data. As a fit to the ring-down profile of $\hat{\psi}_0$ we obtain the frequency $\omega_{\mathrm{fit}} \approx 0.355 + 0.088i$, in agreement with the $l = 2$-mode frequencies $\omega_{l=2mn}$, see [62], which are $\omega_{2-20} \approx 0.34 + 0.089i$, $\omega_{220} \approx 0.36 + 0.089i$, $\cdots$ for our case of $J = 0.3$, $m = 1.035$. After around $t > 90M$ the perturbations on the Kerr background are to weak to be further resolved limited by the total

---

[11] The new techniques could have been implemented directly into the horizon finder, which uses a 6-patch stereographic coordinate system [61]. But to benefit from the exact integration scheme, appendix A, we employ a spherical grid. Both grids a kept at the same resolution.

[12] This new notation denotes that the area A and the three surface integrals $\mu_2(\mathrm{Im}\hat{\Psi}_2)$, $\mu_4(\mathrm{Im}\hat{\Psi}_2)$, $\mu_6(\mathrm{Im}\hat{\Psi}_2)$ are used to determine J_1 as a solution of (4.3).
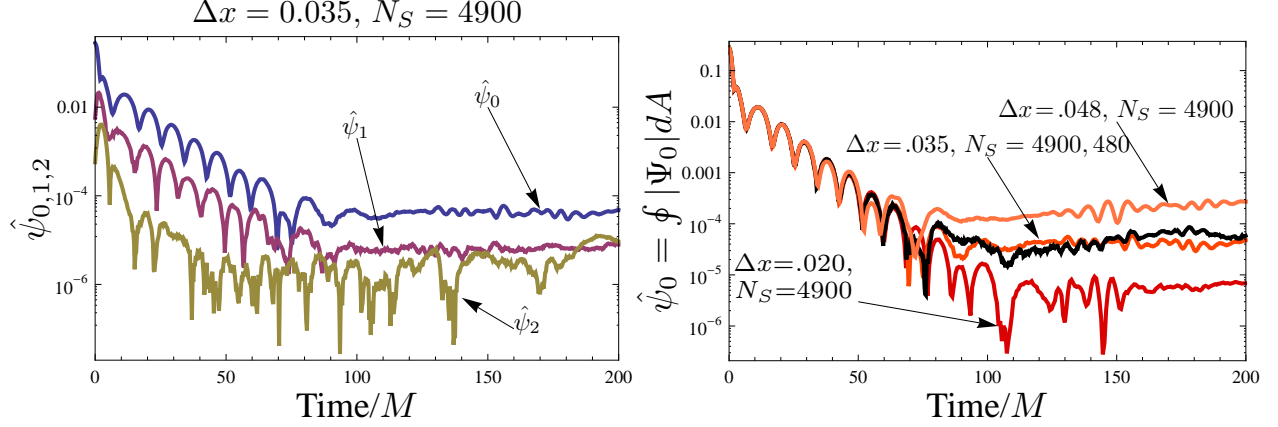
FIG. 1: Left: time evolution of $\hat{\psi}_{1,2,3}$, Right: time evolution of $\hat{\psi}_0$

numerical error, which we downsize by increasing the Cartesian grid resolution, see figure 1 on the right, in order to see the dynamics below $\hat{\psi}_0 < 10^{-5}$. Where the total error [13] is almost independent of the spherical grid resolution and dominated by the error due to time-integrating the BSSN equation. We accomplished this by employing an exact integration scheme (integration over the surface), see appendix A, and the computational techniques of section V.

2. *Evolution and Convergence of the Invariants μ_n*

In figure 2 we see the exponentially damped oscillation of the μ_n as they ring-down to their final Kerr value. On the right it is shown how the time averages of $\mu_2(^2\hat{\mathcal{R}})$ ($120M$-$200M$, straight black lines) converge with the expected 4th-order as the Cartesian grid resolution increases after the oscillations have settled down. Apparently, the error of $\mu_2(^2\hat{\mathcal{R}})$ does not converge uniformly but the effect flattens out as the Cartesian resolution increases.
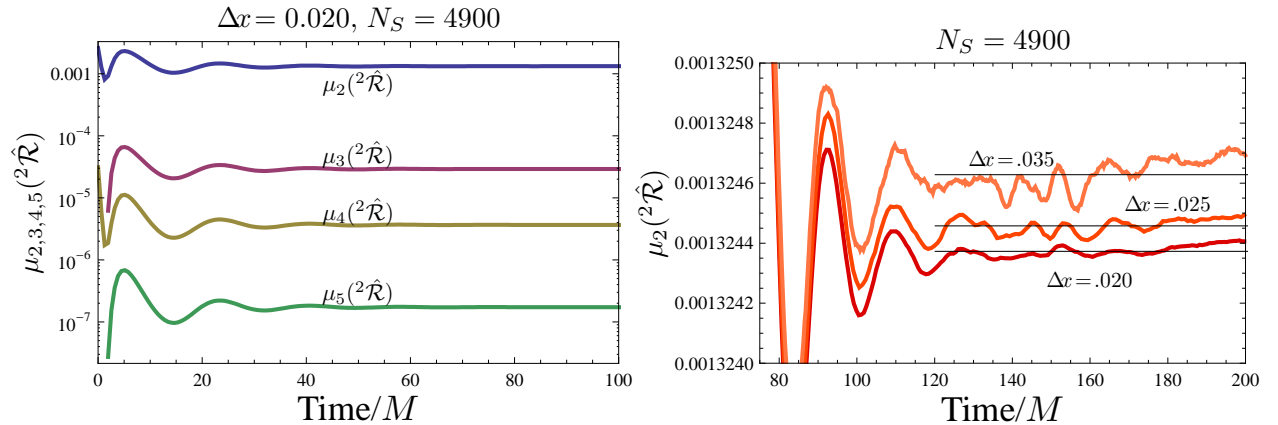

FIG. 2: Left: time evolution of $\mu_{2,3,4,5}(^2\hat{\mathcal{R}})$, Right: time evolution of $\mu_2(^2\hat{\mathcal{R}})$

---

[13] Additional contributions to the total error are due to interpolation and truncation of the series expansion of $h(\theta, \phi)$ at $l_{\max} = 10$ (and due to evaluation).
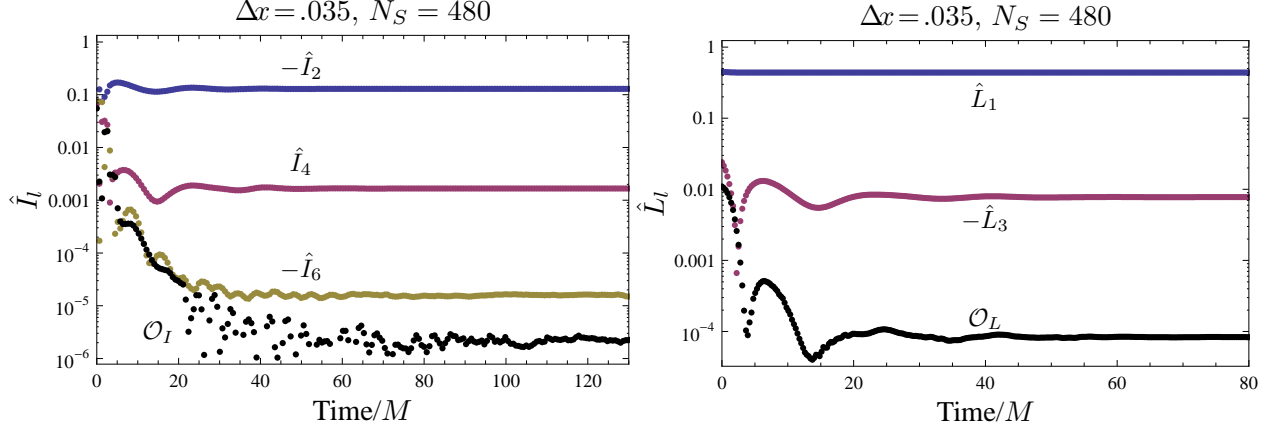
FIG. 3: Left: time evolution of mass $\hat{I}_l$, Right: and angular momentum multipoles moments $\hat{L}_l$

3. Evolution of Mass and Angular Momentum Multipole Moments

Every few time steps the $\mu_n(^2\hat{\mathcal{R}})$, $\mu_n(\mathrm{Im}\hat{\Psi}_2)$ are computed and the algebraic system relating them to the IH multipole moments (assuming reflection- and axisymmetry) is solved, as in the example (4.7), see figure 3, where the $\mathcal{O}_I$, $\mathcal{O}_L$ account for all higher multipole moments. We see that already at $t = 30M$ the assumption of a reflection- and axisymmetric horizon applies, although the AH is still dynamic at that time, see figure 1. Interestingly, $\hat{L}_1$ is almost constant during the evolution, as the horizon area (not plotted, $A \approx 4\pi \cdot 2.05^2 M^2$).

4. Spin Evolution and Comparison with other methods

And finally we show the evolution of the angular momentum dipole $J_1(\mu_{2,4,6}(\mathrm{Im}\hat{\Psi}_2), A)$ [14](red curve) in comparison with other spin measures and approximats, see figure 4 top panels, and their convergence, bottom panels. Here the coordinate approximants $J[\Phi_{\mathrm{asc}}]$, $J[\Phi_{\mathrm{cc}}]$ can be seen as a reference, since we chose the numerical setup conveniently, such that the horizon is 'at rest' (after the dynamical phase) and such that coordinate distortions are small [15]. After a short initial bust all methods yield nearly the same spin value, which stays constant during the evolution; an exception is $J(\mu_2(^2\hat{\mathcal{R}}), A)$ (brown) which oscillates with the quasinormal frequency. This indicates that there is a certain phase in which the horizon is at best modelled by an axisymmetric, dynamical horizon but not Kerr. These 'axisymmetric features' are encoded in the $\mu_{2,4,6}(\mathrm{Im}\hat{\Psi}_2)$ such that we get an overlap of $J_1(\mu_{2,4,6}(\mathrm{Im}\hat{\Psi}_2), A)$ with the references $J[\Phi_{\mathrm{asc}}]$, $J[\Phi_{\mathrm{cc}}]$. The remaining difference $|J[\Phi_{\mathrm{asc}}]/M^2 - 0.3|$ converges with 4th-order as the Cartesian resolution increases, see figure 4 bottom right. Where on the other hand $J[\Phi_{\mathrm{kt}}]$ converges at 2nd-order as the spherical grid resolution increases, bottom left panel [16], because finite differencing on the spherical grid is involved to determine Φ_{kt}^j.

---

[14] This denotes that J_1 is given as a solution of (4.7) and (4.9), where the surface integrals A, $\mu_2(\mathrm{Im}\hat{\Psi}_2)$, $\mu_4(\mathrm{Im}\hat{\Psi}_2)$, $\mu_6(\mathrm{Im}\hat{\Psi}_2)$ were the input.

[15] This is in general not the case in a full BBH simulation.

[16] Note that the low resolution $N_S = 480$ (light blue) is to coarse to be in the convergence regime.
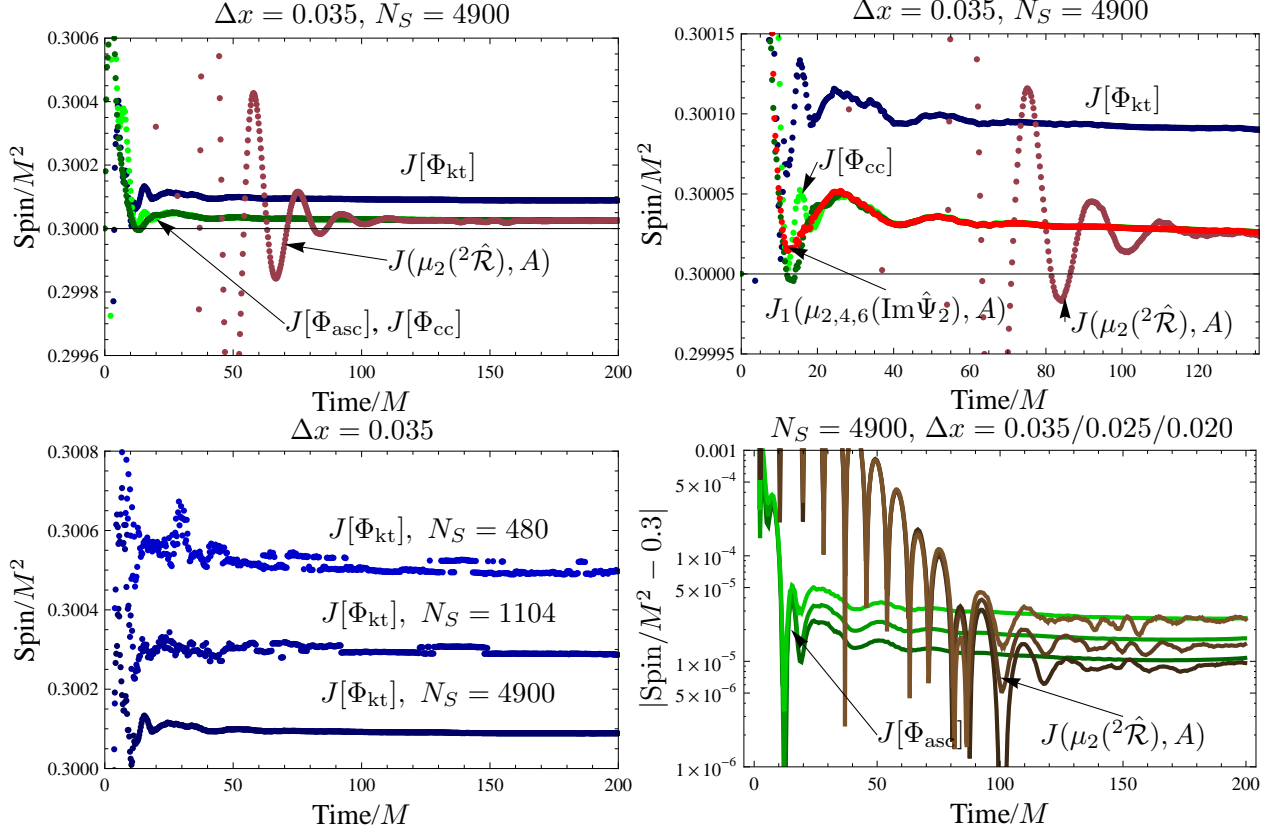
FIG. 4: Top Left: time evolution of other spin measures, Top Right: time evolution of $J_1(\mu_{2,4,6}(\mathrm{Im}\hat{\Psi}_2), A)$ (red) in comparison with other spin measures (zoomed), Bottom Left: convergence of $J[\Phi_{\mathrm{kt}}]$ varying N_S, Bottom Right: convergence of $J[\Phi_{\mathrm{asc}}]$, $J(\mu_2(^2\hat{\mathcal{R}}), A)$ varying Δx

VII. CONCLUSION

The dominant part of the gravitational radiation at Scri is contained in the quadrupole moment of Ψ_4 which is in practice extracted at 'large' coordinate spheres around the source in numerical simulations. Similarly, the dipole moment of the rotational Weyl scalar $\mathrm{Im}\Psi_2$ encodes the quasi-local angular momentum measured at the apparent horizon in the presents of axisymmetry. The local coordinates on the horizon are in general distorted and a solution of the Killing equation is required to determine an invariant coordinates system in which the multipole moments can be computed.

It is involved to determine the Killing vector field, in particular, to find a convenient approximant in case the axisymmetry is perturbed. We have shown a new method to extract the horizon multipole moments using coordinate invariant surface integrals μ_n from which we deduce the multipole moments as a solution of an algebraic system. We have seen that the 'axisymmetric features' contained in the μ_n allow for an accurate quasi-local spin computation, which is the dipole moment solution of this algebraic system. Indeed this angular momentum dipole is equal to the spin (up to numerical errors) given by solutions of the Killing equation, even in the case of a perturbed axisymmetry.

We have also presented the possibility to extract the spin from a single μ_n in comparison with its analytic expression for Kerr. But there seems to be a dynamical phase of the horizon, in which it is

better modeled by an axisymmetric dynamical horizon and not with Kerr. Then the spin extraction by several μ_n is favoured. The perturbations from Kerr oscillate in agreement with black hole perturbation theory, until they are no more resolvable, due to numerical errors. Then the dipole moment of the rotational Weyl scalar agrees with the Kerr spin and the μ_n take their final Kerr value.

The computation of the invariants μ_n is done very accurately using an exact integration scheme. In combination with spectral methods, in order to compute spatial derivatives of the horizon co-ordinate shape function (adapted from horizon finding algorithms), the curvature components $^2\mathcal{R}$, $\text{Im}\Psi_2$ are computed accurately (given the 3+1 evolution variables) and finite differencing on the horizon is avoided. This way we could accomplish that the numerical error of the μ_n (dominated by the time-integration error of the BSSN equations) converges as the Cartesian grid resolution is refined, almost independently of the number of spherical grid points, which can be significantly reduced in order to save computational costs.

Additionally, three technical novelties have been introduced that ease computations on de-formed 2-spheres: an adapted spherical coordinate system (whose azimuthal coordinate vector field can be used to approximate Killing vector fields), the use of a non-standard basis of spherical harmonics and the use of an exact integration scheme. These techniques should be considered for wave extraction on coordinate spheres or constant mean curvature (CMC) spheres [63, 64]. In particular, if Ψ_4 (computed at several coordinate or CMC spheres) is fitted to a polynomial in $1/R_{\text{areal}}$ (and not R_{coord}), for the extrapolation [65].

APPENDIX A: EXACT INTEGRATION SCHEMES FOR SPHERICAL GRIDS

It is well know that the equation

$$\int_a^b f(x)w(x)dx = \sum_{i=1}^N w_i f(x_i) \,, \tag{A1}$$

holds exactly, where $w(x)$ is called the *weight function*, if $f(x)$ is a polynomial of degree less than $2N$ and the weights w_i and abscissas x_i are chosen in accordance with the orthogonal basis of polynomials on $[a, b]$ defined by the scalar product $< f|g >:= \int_a^b f(x)g(x)w(x)\,dx$, because there are $2N$ degrees of freedom to make both sides of (A1) match, see for example [66].

For the integration with $w(x) = 1$ on the circle $a = b$, the 'correct' weights and abscissas are particularly simple. They are N equi-distant points with equal weights. This can not be generalized for the integration on the 2-sphere

$$\oint_{S^2} f(x, y)\,dA = \sum_{i=1}^{N_S} w_i f(x_i, y_i) \,, \tag{A2}$$

for arbitrary N_S, because the number of uniform grid structures is finite $N_S = 4, 6, 8, 12, 20$, corresponding to the faces of the platonic solids. Since this is a 2D integration, we have $3N_S$ degrees of freedom in the sum on the r.h.s. of (A2) and $(l_{\max} + 1)^2$ spherical harmonics of degree $\leq l_{\max}$. This means if $f(x, y)$ was given by an expansion up to $l_{\max}$, we needed at least $N_S = (l_{\max} + 1)^2/3$ points to make (A2) hold. Lets say $f(x)$ was given by an expansion of $(7 + 1)^2 - 4$ spherical harmonics, then the integration (A2) on an icosahedral grid $N_S = 20$ with equal weights would be exact. There is an extensive body of work on the problem of optimal integration schemes for $N_S > 20$ (*cubature problem*), see for example [67].

There are less optimal compromises available, which require much more points than $(l_{\max} + 1)^2/3$, but which are defined on regular spherical (θ, ϕ) grids. For example the Gauss-Legendre/Gauss scheme, where the integration along each interval $[-1, 1]$, $[0; 2\pi]$ is a Gaussian quadrature

$$\oint_0^{2\pi} \int_{-1}^1 f(\chi, \phi) d\chi d\phi = \sum_{i=1}^{N_\chi} \sum_{j=1}^{N_\phi} w_i^\chi w_j^\phi f(\chi_i, \phi_j) , \tag{A3}$$

where again $\chi = \cos\theta$, $N_S = N_\theta \times N_\phi$ and $N_\phi = 2N_\theta$.

As before the ϕ-integration is a Gaussian quadrature for $\phi_j = 2\pi(j - 1)/N_\phi$, $j = 1, ..., N_\phi$ and equal weights $w_j^\phi = 2\pi/N_\phi$, the χ-integration (in that case called Gauss-Legendre quadrature) for χ_i being the roots of the Legendre polynomials (according to the weight function $w(\chi) = 1$). The corresponding weights w_i^χ can be found in e.g. [68]. This method is exact for polynomials of degree less than $2N_\theta$ (less than $\sqrt{2N_S} < \sqrt{3N_S}$).

An alternative integration scheme has been found by [69][17]. There the integration grid is a standard equi-angular (θ, ϕ) grid, $\theta_j = (j - 1/2)\pi/N_\theta$ (staggered) and the computation of the roots of the Legendre polynomials not necessary. The weights for even/odd N_θ are given by

$$w_j^\theta = 4/N_\theta \sum_{k=0}^{N_\theta/2-1} \frac{1}{2l+1} \sin((2k+1)\theta_j) , \quad N_\theta \text{ even}, \tag{A4}$$

$$w_j^\theta = 4/N_\theta \left(\frac{1}{2N_\theta} \sin(N_\theta \cdot \theta_j) + \sum_{k=0}^{(N_\theta-1)/2-1} \frac{1}{2l+1} \sin((2k+1)\theta_j) \right) , \quad N_\theta \text{ odd}, \tag{A5}$$

which allows for exact integration of harmonics of order less than $N_\theta/2$ (less than $\sqrt{1/8N_S} < \sqrt{2N_S} < \sqrt{3N_S}$). Then equation (A3) becomes

$$\oint_0^{2\pi} \int_0^\pi f(\theta, \phi) \sin\theta \, d\theta \, d\phi = \sum_{i=1}^{N_\theta} \sum_{j=1}^{N_\phi} w_i^\theta w_j^\phi f(\theta_i, \phi_j) \sin\theta_j. \tag{A6}$$

A small summarizing example: for the total of $N_S = 512$ we have the cubature limite at $39 \approx \sqrt{3 \cdot 512}$, for the Gauss/Gauss-Legendre scheme we get $l_{\max} < 32$ and for the scheme of [69] we have $l_{\max} < 8$ (which is almost possible on an icosahedral grid [18]with only $N_S = 20$, where $l_{\max} < 8 \approx \sqrt{3 \cdot 20}$).

---

[17] The authors make use of the fact that the points $\chi_j = \cos\theta_j$ (although not the zeros of the Legendre polynomials on $[1; -1]$) are the zeros of the Chebyshev polynomials of the 1st kind.

[18] Therefore, if one is only interested in the first coefficients of a smooth function on the sphere up to $l_{\max} = 6$, an icosahedral grid with equal weights would be a good choice.

FIG. 5: parametrization of the unit-sphere with a shifted spherical coordinate system

APPENDIX B: ADAPTED SPHERICAL COORDINATES

Before solving the 2D Killing equation on a sphere it is useful to have the 2-metric in a convenient coordinate representation, which is 'roughly' adapted to the axisymmetry. Such that the poles of the spherical coordinates system agree with the two minima of the scalar 2-curvature. We assume $^2\mathcal{R}(\theta, \phi)$ to be given on a spherical coordinate system (θ, ϕ), where the two minima are at $N^j = (0, 0, \cos\theta_{\min})$ and $S^j = (0, 0, -\cos\theta_{\min})$, see figure 5. This can always be accomplished by a simple Euler rotation. In order to obtain the adapted spherical coordinates system (θ', ϕ'), we have to shift the Cartesian z-axis along the x-axis by the amount $d := \sin\theta_{\min}$. This is being done by

$$n_j(\theta, \phi) = r'(\theta', \phi')\, n'_j(\theta', \phi') + d \cdot (1, 0, 0)\,, \tag{B1}$$

where $n_j(\theta, \phi) = (\cos\phi\sin\theta, \sin\phi\sin\theta, \cos\theta)$, $n'_j(\theta', \phi') = (\cos\phi'\sin\theta', \sin\phi'\sin\theta', \cos\theta')$ are the radial unit vectors in the corresponding coordinate system. The distance $r'(\theta', \phi')$ is given by

$$r'(\theta', \phi') = \sqrt{d_{\|}^2 - 2r_{\|}d_{\|}\sin\theta + r_{\|}^2}\,, \tag{B2}$$

where $d_{\|}$, $r_{\|}$ are given by

$$r_{\|} = \cos\phi'\cos\phi + |\sin\phi'|\sqrt{1 - \cos^2\phi}\,, \tag{B3}$$
$$d_{\|} = d\cos\phi'\,. \tag{B4}$$

And finally, $\cos\phi$ and $\sin\theta$ in terms of θ', ϕ' are given by

$$\cos\phi = d\sin^2\phi' + \cos\phi'\sqrt{1 - d^2\sin^2\phi'}\,, \tag{B5}$$

$$\sin\theta = \frac{1}{r_{\|}}\left(d_{\|}\cos^2\theta' + \sin\theta'\sqrt{r_{\|}^2 - d^2\cos^2\theta'}\right)\,. \tag{B6}$$

The inverse transformation is given by interchanging $\theta \leftrightarrow \theta'$, $\phi \leftrightarrow \phi'$ $d \leftrightarrow -d$ in the above expressions.

[1] F. Pretorius, Phys. Rev. Lett. **95**, 121101 (2005), gr-qc/0507014.

[2] M. Campanelli, C. O. Lousto, P. Marronetti, and Y. Zlochower, Phys. Rev. Lett. **96**, 111101 (2006), gr-qc/0511048.

[3] J. G. Baker, J. Centrella, D. Choi, M. Koppitz, and J. van Meter, Phys. Rev. D **73**, 104002 (2006), gr-qc/0602026.

[4] M. Campanelli, C. O. Lousto, Y. Zlochower, B. Krishnan, and D. Merritt, Phys. Rev. **D75**, 064030 (2007), gr-qc/0612076.

[5] M. Campanelli, C. O. Lousto, H. Nakano, and Y. Zlochower (2008), 0808.0713.

[6] L. Rezzolla et al., Astrophys. **J679**, 1422 (2008), 0708.3999.

[7] L. Rezzolla et al., Astrophys. J. **674**, L29 (2008), 0710.3345.

[8] E. Barausse and L. Rezzolla (2009), 0904.2577.

[9] W. Tichy and P. Marronetti, Phys. Rev. **D78**, 081501 (2008), 0807.2985.

[10] L. Boyle and M. Kesden, Phys. Rev. **D78**, 024017 (2008), 0712.2819.

[11] D. Pollney et al., Phys. Rev. **D76**, 124002 (2007), arXiv:0707.2559 [gr-qc].

[12] J. G. Baker et al., Phys. Rev. **D78**, 044046 (2008), 0805.1428.

[13] F. Herrmann, I. Hinder, D. M. Shoemaker, P. Laguna, and R. A. Matzner, Phys. Rev. **D76**, 084032 (2007), 0706.2541.

[14] P. Marronetti, W. Tichy, B. Bruegmann, J. Gonzalez, and U. Sperhake, Phys. Rev. **D77**, 064010 (2008), 0709.2160.

[15] M. Campanelli, C. O. Lousto, and Y. Zlochower, Phys. Rev. **D74**, 084023 (2006), astro-ph/0608275.

[16] M. A. Scheel et al., Phys. Rev. **D79**, 024003 (2009), 0810.1767.

[17] M. Shibata and K. Taniguchi, Phys. Rev. **D73**, 064027 (2006), astro-ph/0603145.

[18] K. Kiuchi, Y. Sekiguchi, M. Shibata, and K. Taniguchi (2009), 0904.4551.

[19] M. Shibata, Prog. Theor. Phys. **101**, 1199 (1999), gr-qc/9905058.

[20] J. Font, Living Reviews in Relativity **11** (2008).

[21] L. Baiotti, B. Giacomazzo, and L. Rezzolla, Phys. Rev. **D78**, 084033 (2008), 0804.0594.

[22] M. Shibata and K. Uryu, Phys. Rev. **D74**, 121503 (2006), gr-qc/0612142.

[23] Z. B. Etienne et al., Phys. Rev. **D77**, 084002 (2008), 0712.2460.

[24] M. D. Duez et al., Phys. Rev. **D78**, 104015 (2008), 0809.0002.

[25] M. Shibata, Phys. Rev. D **67**, 024033 (2003).

[26] M. Shibata, T. W. Baumgarte, and S. L. Shapiro, Phys. Rev. D **61**, 044012 (2000).

[27] L. Baiotti et al., Phys. Rev. **D71**, 024035 (2005), gr-qc/0403029.

[28] L. Baiotti and L. Rezzolla, Phys. Rev. Lett. **97**, 141101 (2006), gr-qc/0608113.

[29] A. Ashtekar, S. Fairhurst, and B. Krishnan, Phys. Rev. **D62**, 104025 (2000), gr-qc/0005083.

[30] A. Ashtekar, C. Beetle, and J. Lewandowski, Phys. Rev. D **64**, 044016 (2001).

[31] A. Ashtekar and B. Krishnan, Living Rev. Rel. **7**, 10 (2004), gr-qc/0407042.

[32] A. Ashtekar and B. Krishnan, Phys. Rev. Lett. **89**, 261101 (2002).

[33] O. Dreyer, B. Krishnan, D. Shoemaker, and E. Schnetter, Phys. Rev. **D67**, 024018 (2003), gr-qc/0206008.

[34] G. Cook and B. Whiting, Physical Review D **76**, 41501 (2007).

[35] R. Matzner, Journal of Mathematical Physics **9**, 1657 (2003).

[36] L. Smarr, Physical Review D **7**, 289 (1973).

[37] A. Ashtekar, J. Engle, T. Pawlowski, and C. Van Den Broeck, Class. Quant. Grav. **21**, 2549 (2004),

gr-qc/0401114.

[38] I. Booth, Can. J. Phys. **83**, 1073 (2005), gr-qc/0508107.

[39] E. Gourgoulhon and J. L. Jaramillo, Phys. Rept. **423**, 159 (2006), gr-qc/0503113.

[40] T. Baumgarte, G. Cook, M. Scheel, S. Shapiro, and S. Teukolsky, Physical Review D **54**, 4849 (1996).

[41] G. Wald, *General relativity* (Chicago, 1984).

[42] G. Lovelace, R. Owen, H. Pfeiffer, and T. Chu, Arxiv preprint arXiv:0805.4192 (2008).

[43] M. Caudill, G. Cook, J. Grigsby, and H. Pfeiffer, Physical Review D **74**, 64011 (2006).

[44] C. Beetle (2008), 0808.1745.

[45] L. Smarr, Phys. Rev. D **7**, 289 (1973).

[46] S. Chandrasekhar, *The Mathematical Theory of Black Holes* (Oxford University Press, Oxford, England, 1983).

[47] J. Thornburg, Living Reviews in Relativity (2007).

[48] K. S. Thorne, Rev. Mod. Phys. **52**, 299 (1980).

[49] B. M. Project, A. Erdélyi, H. Bateman, and E. U. O. of Naval Research, *Higher Transcendental Functions* (McGraw-Hill, 1953).

[50] M. Lachieze-Rey, Journal of Physics A Mathematical and General **37**, 205 (2004).

[51] B. Kelly (2004), the May Project: The Newman-Penrose Scalars.

[52] L. Smarr, Ph. D. Thesis Texas Univ., Austin. (1975).

[53] G. Allen, W. Benger, T. Goodale, H. Hege, G. Lanfermann, A. Merzky, T. Radke, E. Seidel, and J. Shalf, in *High-Performance Distributed Computing, 2000. Proceedings. The Ninth International Symposium on* (2000), pp. 253–260.

[54] S. Brandt and B. Bruegmann, Phys. Rev. Lett. **78**, 3606 (1997), gr-qc/9703066.

[55] M. Ansorg, B. Bruegmann, and W. Tichy, Phys. Rev. **D70**, 064011 (2004), gr-qc/0404056.

[56] T. Nakamura, K. Oohara, and Y. Kojima, Prog. Theor. Phys. Suppl. **90**, 1 (1987).

[57] M. Shibata and T. Nakamura, Phys. Rev. D **52**, 5428 (1995).

[58] T. W. Baumgarte and S. L. Shapiro, Phys. Rev. D **59**, 024007 (1998), gr-qc/9810065.

[59] M. Alcubierre et al., Phys. Rev. **D67**, 084023 (2003), gr-qc/0206072.

[60] E. Schnetter, CARPET: A Mesh Refinement driver for CACTUS.

[61] J. Thornburg, Phys. Rev. D **54**, 4899 (1996), gr-qc/9508014.

[62] E. W. Leaver, Proc. Roy. Soc. Lond. **A402**, 285 (1985).

[63] E. Schnetter, Class. Quant. Grav. **20**, 4719 (2003), gr-qc/0306006.

[64] J. Metzger, Class. Quant. Grav. **21**, 4625 (2004), gr-qc/0408059.

[65] M. Boyle and A. H. Mroue (2009), 0905.3177.

[66] G. Szegö, American Mathematical Society, New York (1939).

[67] S. Sobolev, *Introduction to the Theory of Cubature Formulae* (Moscow: NAUKA, 1974).

[68] W. Press, S. Teukolsky, B. Flannery, and W. Vetterling, *Numerical Recipes: FORTRAN* (Cambridge University Press New York, NY, USA, 1990).

[69] J. Driscoll and D. Healy Jr, Advances in Applied Mathematics **15**, 202 (1994).